Journal of Molecular Graphics and Modelling 27 (2009) 978–982

Contents lists available at ScienceDirect

Journal of Molecular Graphics and Modelling

journal homepage: www.elsevier.com/locate/JMGM

Short communication

Comparison of computational approaches for predicting the effects of missense mutations on p53 function

Lillian T. Chong [a,*], Jed W. Pitera [b], William C. Swope [b], Vijay S. Pande [c]

[a] Department of Chemistry, University of Pittsburgh, Pittsburgh, PA 15260, United States
[b] IBM Almaden Research Center, San Jose, CA 95120, United States
[c] Department of Chemistry, Stanford University, Stanford, CA 94305, United States

ARTICLE INFO

Article history:
Received 23 July 2008
Received in revised form 17 December 2008
Accepted 18 December 2008
Available online 27 December 2008

Keywords:
Computational mutagenesis
Tumor suppressor p53
Missense mutations
Distributed computing

ABSTRACT

We applied our recently developed kinetic computational mutagenesis (KCM) approach [L.T. Chong, W.C. Swope, J.W. Pitera, V.S. Pande, Kinetic computational alanine scanning: application to p53 oligomerization, J. Mol. Biol. 357 (3) (2006) 1039–1049] along with the MM-GBSA approach [J. Srinivasan, T.E. Cheatham 3rd, P. Cieplak, P.A. Kollman, D.A. Case, Continuum solvent studies of the stability of DNA, RNA, and phosphoramidate-DNA helices, J. Am. Chem. Soc. 120 (37) (1998) 9401–9409; P.A. Kollman, I. Massova, C.M. Reyes, B. Kuhn, S. Huo, L.T. Chong, M. Lee, T. Lee, Y. Duan, W. Wang, O. Donini, P. Cieplak, J. Srinivasan, D.A. Case, T.E. Cheatham 3rd., Calculating structures and free energies of complex molecules: combining molecular mechanics and continuum models, Acc. Chem. Res. 33 (12) (2000) 889–897] to evaluate the effects of all possible missense mutations on dimerization of the oligomerization domain (residues 326–355) of tumor suppressor p53. The true positive and true negative rates for KCM are comparable (within 5%) to those of MM-GBSA, although MM-GBSA is much less computationally intensive when it is applied to a single energy-minimized configuration per mutant dimer. The potential advantage of KCM is that it can be used to directly examine the *kinetic* effects of mutations.

© 2008 Elsevier Inc. All rights reserved.

1. Introduction

Mutagenesis of specific residues in proteins has proven invaluable in probing the contributions of individual amino acid side-chains to the biological functions of proteins. For example, alanine scanning mutagenesis, a method of systematic alanine substitution, has revealed critical residues for protein–protein interactions [4], enzyme activity [5], and protein stability [6]. High-throughput mutagenesis approaches are also useful tools for the construction of protein–protein interaction networks, characterization of disease-linked mutations, and protein design.

As a more efficient alternative to laboratory mutagenesis approaches when structures are available, computational approaches based on both thermodynamic [7–11] and kinetic [1] analyses have been developed in recent years. The latter is our kinetic computational mutagenesis (KCM) approach [1], which involves analysis of ensemble unfolding kinetics at high temperature using molecular dynamics (MD) simulations [1]. We applied this approach to dimerization of the oligomerization domain of tumor suppressor p53 (p53tet), an intermediate step to forming the biologically active tetramer [12]. Given that over half of human cancers are linked to mutations in p53 [13,14], high-throughput analysis of mutations in all domains of p53, including p53tet, is of great biomedical interest. As validated by experimental results [15], our approach, when used for *in silico* alanine scanning, identifies deleterious mutations in p53tet with reasonable success [1]. In other words, residues that were identified to be critical for dimer unfolding kinetics were generally thermodynamically important as well.

Here we have used KCM to perform more extensive mutagenesis of p53tet, analyzing the effects of all possible single-nucleotide polymorphisms, or missense mutations, at each residue position. Our resulting predictions of mutations that inactivate p53 are compared to those identified based on impaired transcriptional activity in a yeast-based assay [16]. To evaluate the cost-effectiveness of KCM, which requires about a week of simulation time on 100 independent CPUs per mutant dimer, we also carried out computational mutagenesis using MM-GBSA [2,3] for comparison. In contrast to KCM, MM-GBSA requires only seconds on a single CPU when applied to a single energy-minimized configuration per mutant dimer.

* Corresponding author. Tel.: +1 412 624 6026.
E-mail address: ltchong@pitt.edu (L.T. Chong).

1093-3263/$ – see front matter © 2008 Elsevier Inc. All rights reserved.
doi:10.1016/j.jmgm.2008.12.006

2. Methods

2.1. Simulation details

Model building and simulations were performed using the GROMACS MD software package [17] modified for the Folding@Home distributed computing infrastructure [18]. Coordinates of heavy atoms were taken from the crystal structure of p53tet (1AIE in the Protein Data Bank) [19] in its active tetrameric form to create a starting model of the wild-type dimer. The NCBI GenBank X54156 sequence for wild-type p53tet was used to determine all possible missense mutations (a total of 177). Heavy atoms for residue mutations, affecting both monomers, were positioned using the SCAP side-chain prediction program in the Jackal 1.5 protein structure modeling software package [20]. Acetyl and *N*-methyl capping groups were added to the N-terminus and C-terminus, respectively, of each monomer (residues 326–355). Hydrogens were added using ionization states present in neutral solution. Neutral histidine residues were protonated at the ε-nitrogen, the predominant tautomer for free histidines in solution [21]. The dimer was solvated in a cubic box of TIP3P water [22] with an initial box length of 50 Å, then charge neutralized by adding counterions. MD simulations were performed at constant temperature and pressure (1 atm) using the modified AMBER ff94 force field developed by Garcia and Sonbanmatsu (AMBER-GS) [23]. Further simulation details are discussed in Chong et al. [1].

To relieve unfavorable interactions, each initial model was subjected to energy minimization followed by equilibration in two stages. The first stage of equilibration involved a 1 ns MD simulation of the solvent and counterions at 300 K with the protein constrained. In the second stage, 100 independent 1 ns MD simulations of the entire system at 300 K with different initial velocities (selected from a Maxwell–Boltzmann distribution at 300 K) were run in parallel on the Folding@Home distributed computing network [18]. Each of these independent trajectories was then simulated at 470 K for 20 ns in order to rapidly unfold the dimer, yielding ∼2 μs of aggregate simulation data for each mutant dimer.

2.2. Determination of unfolding rates

Definitions for the unfolded and folded manifold were taken from Chong et al. [24]. These definitions involve the root-mean-squared deviation (RMSD) of C^{α} atoms from the initial dimer structure for all atoms and for the subset of atoms in the β-sheet region. Fitting for RMSD calculations was performed using the quaternion superposition algorithm [25] as implemented in the program ProFit [26]. For each mutant dimer, the increase in the ensemble fraction unfolded $f_u(t)$ as a function of time (t) can be described for $t > t_0$ by a single exponential function with a lag time (t_0)

$$f_u(t) = 1 - e^{-k_u(t-t_0)} \tag{1}$$

where k_u is the rate constant for unfolding at 470 K. The ensemble fraction unfolded was determined every 200 ps from simulations of the mutant dimer at 470 K, yielding one sigma uncertainties $\sigma[f_u(t)]$ that are ∼0.05 or less according to a binomial distribution

$$\sigma[f_u(t)] = \sqrt{\frac{f_u(t)[1 - f_u(t)]}{N_{tot}}} \tag{2}$$

where N_{tot} is the total number of unfolding simulations (*i.e.* 100). To estimate the unfolding rate constant (k_u) at 470 K based on the long timescale events, as opposed to the short-timescale events represented by the lag portion ($t < t_0$) of the data, the natural logarithm of both sides of Eq. (1) was taken

$$\ln[1 - f_u(t)] = -k_u t + k_u t_0 \tag{3}$$

allowing k_u to be determined from a weighted linear least squares fit [27]. Uncertainties $\sigma[f_u(t)]/[1 - f_u(t)]$ in the $\ln[1 - f_u(t)]$ values were used to compute the weights in the fit. Further details about the fitting procedure and determination of the uncertainty in the estimated unfolding rate constant are described in Chong et al. [1].

2.3. Calculation of binding free energies

To compute the binding free energy for the rigid monomer–monomer associations to form each dimer, MM-GBSA free energy calculations [2,3] were performed on monomer and dimer conformations taken from a dimer structure that has been energy-minimized according to the protocol described above. The binding free energy of a mutant dimer relative to the wild-type dimer ($\Delta\Delta G_{bind}$) is approximated as follows:

$$\Delta\Delta G_{bind} = \Delta G_{bind}(mut) - \Delta G_{bind}(wt) \tag{4}$$

$$\begin{aligned} \Delta G_{bind} &= G_{bind,dimer} - G_{bind,\ monomer\ A} - G_{bind,\ monomer\ B} \\ \Delta G_{bind} &\cong (E_{MM,\ dimer} - E_{MM,\ monomer\ A} - E_{MM,\ monomer\ B}) \\ &\quad + (G_{solv,\ dimer} - G_{solv,\ monomer\ A} - G_{solv,\ monomer\ B}) \\ &\quad - (TS_{dimer} - TS_{monomer\ A} - TS_{monomer\ B}) \\ \Delta G_{bind} &= \Delta E_{MM} + \Delta G_{solv} - T\Delta S \end{aligned} \tag{5}$$

$$\Delta E_{MM} = \Delta E_{elec} + \Delta E_{vdW} + \Delta E_{int} \tag{6}$$

$$\Delta G_{solv} = \Delta G_{GB} + \Delta G_{SA} \tag{7}$$

where ΔE_{MM} is the change in the total molecular mechanical energy of the solute with an electrostatic component (ΔE_{elec}), a van der Waals component (ΔE_{vdW}), and an internal component (ΔE_{int}) consisting of bond, angle, and torsional energies determined using the AMBER-GS force field [23]; ΔG_{solv} is the solvation energy difference, which consists of an electrostatic contribution (ΔG_{GB}) determined by using a modified Generalized Born model [28,29] and a nonpolar contribution (ΔG_{SA}) that is linearly dependent on the change in solvent-accessible surface area (ΔSASA); $-T\Delta S$ is the solute entropic contribution to the binding free energy. Because the same monomer configurations are used for their respective unbound and bound states, ΔE_{int} is always equal to zero. The electrostatic contribution to the solvation free energy (ΔG_{GB}) was computed using a set of three different internal dielectric constants, depending on the type of amino acid residue: 2 for nonpolar residues, 3 for polar residues, and 4 for charged residues. The use of these different constants accounts for the different degrees of protein structural relaxation that result when different types of amino acid residues are mutated, and has been shown to dramatically improve the accuracy of computed $\Delta\Delta G_{bind}$'s using the MM-PBSA approach (same as MM-GBSA, but using the Poisson–Boltzmann model instead of a Generalized Born model) [10,11]. Nonpolar contributions to solvation free energies (ΔG_{SA}) were computed according to the following relation: $\Delta G_{SA} = \gamma\Delta SASA$, where $\gamma = 0.0072$ kcal/Å^2 mol, as recommended for use with AMBER charges [30], and ΔSASA is computed using the LCPO method [31]. Solute entropic contributions were not calculated in this study since they are only crudely estimated by normal mode analysis and likely to be similar for all the dimers.

3. Results and discussion

To compare the cost-effectiveness of KCM [1] and MM-GBSA [2,3] in identifying deleterious mutations in p53tet, we used a common starting model for the wild-type p53tet dimer that was taken from the crystal structure of the tetramer. As discussed in

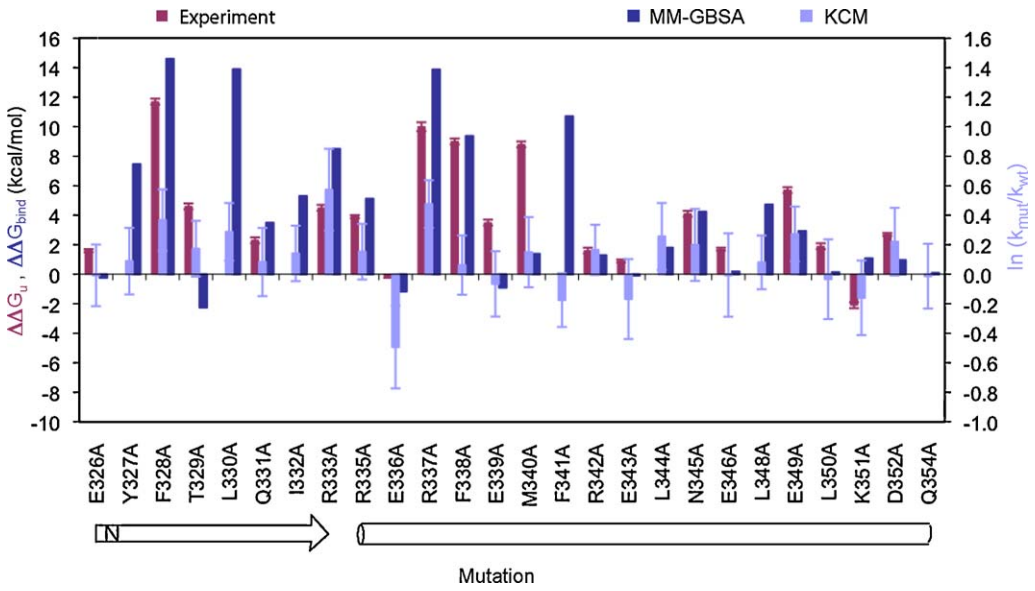

Fig. 1. Qualitative comparison of alanine scanning results from computational vs. experimental approaches. KCM results have been previously published in Chong et al. [1] and are reported as mutation-induced changes in the height of the unfolding barrier as estimated by $\ln(k_{mut}/k_{wt})$ for the p53tet dimer. MM-GBSA results are binding free energies of the mutant dimer relative to the wild-type dimer ($\Delta\Delta G_{bind}$'s). Experimental results are the free energies of unfolding the mutant p53tet tetramer relative to the wild-type p53tet tetramer ($\Delta\Delta G_u$'s) at a denaturant concentration that leads to ~50% unfolding [14]. Standard deviations for the KCM results were determined as described in Section 2. No standard deviations are shown for the MM-GBSA results since only a single calculation was performed for each mutant dimer. Uncertainties shown for the experimental results are the standard errors of fitting [14]. No experimental values are available for Y327A, L330A, I332A, F341A, L344A, L348A, and Q354A for reasons discussed in Mateu and Fersht [15].

our previous paper, a dimer model was used rather than a tetramer model for a greater likelihood of identifying thermodynamically destabilizing mutations with kinetic analyses [1]. While use of this model prevents us from identifying mutations that destabilize the tetramer, but have little effect on the dimer, mutations that destabilize the dimer are also expected to destabilize the tetramer.

3.1. Alanine scanning

KCM and MM-GBSA were first compared in terms of identifying deleterious mutations through alanine scanning. To determine whether a mutation is stabilizing or destabilizing using KCM [1], the mutation's effect on the height of the barrier to unfolding was estimated by $\ln(k_{mut}/k_{wt})$. Using the MM-GBSA approach [2,3], the mutation's effect on the binding free energy upon dimer formation ($\Delta\Delta G_{bind}$) was computed. Results from both KCM ($\ln(k_{mut}/k_{wt})$; previously published by Chong et al. [1]) and MM-GBSA ($\Delta\Delta G_{bind}$) calculations were evaluated as possible indicators of deleterious mutations by comparison with mutation-induced changes in the free energies of tetramer unfolding ($\Delta\Delta G_u$) using CD spectroscopy and guanidinium hydrochloride as a denaturant [15]. It is not possible to quantitatively compare all three sets of data due to differences in the nature of the analysis (kinetic vs. thermodynamic), the denaturant used (thermal vs. chemical), and the oligomerization state of p53tet being considered (dimer vs. tetramer). However, as shown in Fig. 1, it is clear that both the KCM and MM-GBSA results qualitatively agree with the experimentally measured results in terms of the *sign* of the mutation-induced change in free energy [1].

3.2. Missense mutations

Results from KCM and MM-GBSA for all possible p53tet missense mutations are compared to experimental data in terms of the fraction of possible missense mutations at each residue position that are determined to be deleterious. Using the KCM approach [1], mutations were considered deleterious if the unfolding rate constants minus one standard deviation for the resulting mutant dimers are faster than that for the wild-type dimer ($0.11 \pm 0.02\ ns^{-1}$). Using MM-GBSA [2,3], deleterious mutations were defined as ones that destabilized the dimer by more than 2 kcal/mol, the same threshold used by Moreira et al. [10,11] to distinguish "null-spot" mutations from those representing "warm-spots" or "hot-spots" for binding. Using the experimental data [16,32], mutations were considered deleterious if the standardized intensities of transcriptional activity were ≤ -0.5 for at least six out of eight p53 target promoters.

As shown in Fig. 2, KCM and MM-GBSA generally agree in their predictions of the fraction of possible missense mutations that are deleterious at a given residue position. In fact, the percentages of true positives and true negatives for individual mutations that are predicted to be deleterious are comparable for both approaches despite the dramatic difference in computational cost (Table 1). The percentages of true positives for KCM and MM-GBSA are 58 and 63%, respectively, while the percentages of true negatives are higher (76 and 72%, respectively). Thus, these computational approaches appear to be more successful at filtering out mutations that have little effect on p53tet dimerization than at identifying all possible deleterious mutations. Some of the false negatives are mutations that involve residues at the tetramer interface (A347 and K351), which may have little effect on the dimerization step examined by the computational approaches. It is also worth noting that the

Table 1
Success and efficiency of KCM and MM-GBSA.

	MM-GBSA	KCM
% true positives	63	58
% true negatives	72	76
CPU hours/mutant	~0.002	~188

The CPU time per mutant is approximated by the time required to evaluate the wild-type p53tet dimer on a 2.8 gHz Intel processor. In the MM-GBSA approach, this time consists of energy-minimizing the dimer, and evaluating the MM-GBSA energies of the monomer and dimer. In our unfolding simulations approach, the CPU time consists of carrying out 100 20-ns unfolding simulations of the dimer and determining the unfolding rate constant from the resulting simulation data. The percentages of true positives and true negatives are determined relative to the experimental data.

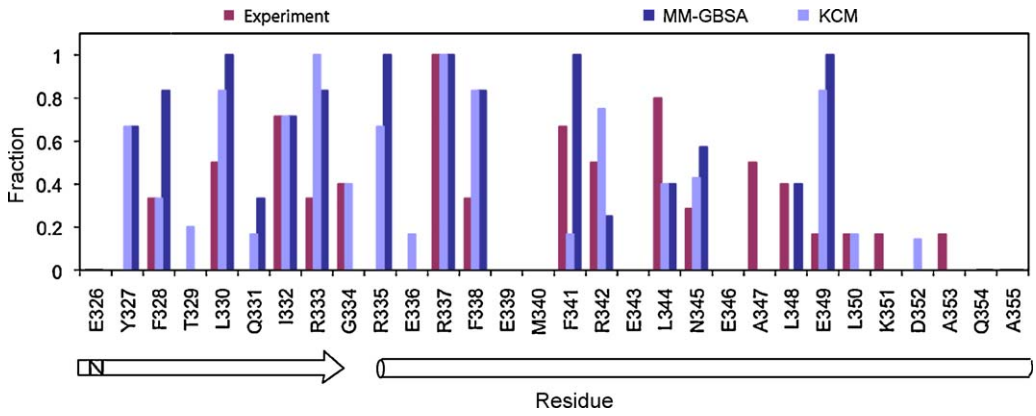

Fig. 2. Deleterious mutations determined by KCM, MM-GBSA, and experiment. Using the KCM, mutations were considered deleterious if their unfolding rate constants minus one standard deviation were faster than that for the wild-type p53tet dimer ($0.11 \pm 0.02\ ns^{-1}$). Using MM-GBSA [2,3], deleterious mutations were defined as those that destabilized the dimer by more than 2 kcal/mol. Using the experimental data [16,32], mutations were considered deleterious if the standardized intensities of transcriptional activity were ≤ -0.5 for at least six out of eight p53 target genes.

degree of p53tet stability does not necessarily correlate with the level of p53 transcriptional activity [32]. Ideally, measured thermodynamic and/or kinetic effects of each missense mutation should be used to validate our computational results, but these measurements have not yet been reported. No correlation appears to exist between the chemical properties of a mutation (residue type, hydrophobicity, etc.) and its tendency to be a true positive or negative prediction (additional data in Supporting Information).

4. Conclusion

In conclusion, we have used our recently developed KCM approach [1] to evaluate the effects of all possible missense mutations in p53tet on its unfolding kinetics at high-temperature. In terms of identifying mutations that inactivate p53, our approach does not perform significantly better than the thermodynamic MM-GBSA approach [2,3], which is much less computationally intensive when it involves only energy-minimized structures. It is evident from these results that MM-GBSA would be the preferable computational approach for the high-throughput evaluation of mutation since it can be run in a trivial amount of time (~6 s per mutant) on a typical PC. This comparison underscores the importance of evaluating the value of new approaches that utilize large computational resources (e.g. distributed computing or parallel supercomputers) in reference to much less computationally intensive approaches. KCM, although not the preferable approach for predicting the thermodynamic-related effects of mutations, provides a means to directly examine the *kinetic* effects of mutations.

Acknowledgements

We thank the Folding@Home volunteers who made this work possible. We also thank Chikashi Ishioka at Tohoku University in Japan for sending us the standardized data from their yeast-based functional assay on p53. This work was supported by grants from NSF Molecular Biophysics and CPIMA (an NSF MRSEC). The distribution of computed $\Delta\Delta G_{bind}$'s, k_u's, and a list of mutations predicted to be deleterious by KCM and MM-GBSA are provided in Supporting Information.

Appendix A. Supplementary data

Supplementary data associated with this article can be found, in the online version, at doi:10.1016/j.jmgm.2008.12.006.

References

[1] L.T. Chong, W.C. Swope, J.W. Pitera, V.S. Pande, Kinetic computational alanine scanning: application to p53 oligomerization, J. Mol. Biol. 357 (3) (2006) 1039–1049.
[2] J. Srinivasan, T.E. Cheatham 3rd, P. Cieplak, P.A. Kollman, D.A. Case, Continuum solvent studies of the stability of DNA, RNA, and phosphoramidate-DNA helices, J. Am. Chem. Soc. 120 (37) (1998) 9401–9409.
[3] P.A. Kollman, I. Massova, C.M. Reyes, B. Kuhn, S. Huo, L.T. Chong, M. Lee, T. Lee, Y. Duan, W. Wang, O. Donini, P. Cieplak, J. Srinivasan, D.A. Case, T.E. Cheatham 3rd, Calculating structures and free energies of complex molecules: combining molecular mechanics and continuum models, Acc. Chem. Res. 33 (12) (2000) 889–897.
[4] J.A. Wells, Systematic mutational analysis of protein–protein interfaces, Methods Enzymol. 202 (1991) 390–411.
[5] C.S. Gibbs, M.U. Zoller, Identification of electrostatic interactions that determine the phosphorylation site specificity of the cAMP-dependent protein kinase, Biochemistry 30 (22) (1991) 5329–5334.
[6] M. Blaber, W.A. Baase, N. Gassner, B.W. Matthews, Alanine scanning mutagenesis of the alpha-helix 115–123 of phage T4 lysozyme: effects on structure, stability, and the binding of solvent, J. Mol. Biol. 246 (2) (1995) 317–330.
[7] I. Massova, P.A. Kollman, Computational alanine scanning to probe protein–protein interactions: a novel approach to evaluate binding free energies, J. Am. Chem. Soc. 121 (36) (1999) 8133–8143.
[8] T. Kortemme, D. Baker, A simple physical model for binding energy hot spots in protein–protein complexes, Proc. Natl. Acad. Sci. U.S.A. 99 (22) (2002) 14116–14121.
[9] R. Guerois, J.E. Nielsen, L. Serrano, Predicting changes in the stability of protein and protein complexes: a study of more than 1000 mutations, J. Mol. Biol. 320 (2) (2002) 369–387.
[10] I.S. Moreira, P.A. Fernandes, M.J. Ramos, Unravelling hot spots: a comprehensive computational mutagenesis study, Theor. Chem. Acc. 117 (2007) 99–113.
[11] I.S. Moreira, P.A. Fernandes, M.J. Ramos, Computational alanine scanning mutagenesis—an improved methodological approach, J. Comput. Chem. 28 (2006) 644–654.
[12] M.G. Mateu, M.M. Sanchez Del Pino, A.R. Fersht, Mechanism of folding and assembly of a small tetrameric protein domain from tumor suppressor p53, Nat. Struct. Biol. 6 (2) (1999) 191–198.
[13] M. Hollstein, D. Sidransky, B. Vogelstein, C.C. Harris, p53 mutations in human cancers, Science 253 (5015) (1991) 49–53.
[14] A.J. Levine, M.C. Wu, A. Chang, A. Silver, E.F. Attiyeh, J. Lin, C.B. Epstein, The spectrum of mutations at the p53 locus, Ann. N.Y. Acad. Sci. 768 (1995) 111–128.
[15] M.G. Mateu, A.R. Fersht, Nine hydrophobic side chains are key determinants of the thermodynamic stability and oligomerization status of tumor suppressor p53 tetramerization domain, EMBO J. 17 (10) (1998) 2748–2758.
[16] S. Kato, S.Y. Han, W. Liu, K. Otsuka, H. Shibata, R. Kanamaru, C. Ishioka, Understanding the function-structure and function-mutation relationships of p53 tumor suppressor protein by high-resolution missense mutation analysis, Proc. Natl. Acad. Sci. U.S.A. 100 (14) (2003) 8424–8429.
[17] E. Lindahl, B. Hess, D. van der Spoel, GROMACS 3.0: a package for molecular simulation and trajectory analysis, J. Mol. Model. 7 (8) (2001) 306–317.
[18] V.S. Pande, I. Baker, J. Chapman, S.P. Elmer, S. Khaliq, S.M. Larson, Y.M. Rhee, M.R. Shirts, C.D. Snow, E.J. Sorin, B. Zagrovic, Atomistic protein folding simulations on the submillisecond time scale using worldwide distributed computing, Biopolymers 68 (1) (2003) 91–109.
[19] P.R. Mittl, P. Chene, M.G. Grutter, Crystallization and structure solution of p53 (residues 326–356) by molecular replacement using an NMR model as template, Acta Crystallogr. D: Biol. Crystallogr. 54 (Pt 1) (1998) 86–89.
[20] Z. Xiang, B. Honig, Extending the accuracy limits of prediction for side-chain conformations, J. Mol. Biol. 311 (2) (2001) 421–430.

[21] M. Tanokura, M. Tasumi, T. Miyazawa, 1H nuclear magnetic resonance studies of histidine-containing di- and tripeptides. Estimation of the effects of charged groups on the pKa value of the imidazole ring, Biopolymers 15 (2) (1976) 393–401.
[22] W. Jorgensen, J. Chandrasekhar, J. Madura, R. Impey, M. Klein, Comparison of simple potential functions for simulating liquid water, J. Chem. Phys. 79 (2) (1983) 926–935.
[23] A.E. Garcia, K.Y. Sanbonmatsu, Alpha-helical stabilization by side chain shielding of backbone hydrogen bonds, Proc. Natl. Acad. Sci. U.S.A. 99 (5) (2002) 2782–2787.
[24] L.T. Chong, C.D. Snow, Y.M. Rhee, V.S. Pande, Dimerization of the p53 oligomerization domain: identification of a folding nucleus by molecular dynamics simulations, J. Mol. Biol. 345 (4) (2005) 869–878.
[25] A.D. McLachlan, Rapid comparison of protein structures, Acta Crystallogr. A 38 (1982) 871–873.
[26] A.C.R. Martin, http://www.bioinf.org.uk/software/profit/.
[27] J.R. Taylor, An Introduction to Error Analysis: The Study of Uncertainties in Physical Measurements, University Science Books, Mill Valley, CA, 1997, p. 327.
[28] A. Onufriev, D. Bashford, D.A. Case, Modification of the generalized born model suitable for macromolecules, J. Phys. Chem. B 104 (15) (2000) 3712–3720.
[29] A. Onufriev, D. Bashford, D.A. Case, Exploring protein native states and large-scale conformational changes with a modified generalized born model, Proteins 55 (2) (2004) 383–394.
[30] W.C. Still, A. Tempczyk, R.C. Hawley, T. Hendrickson, Semianalytical treatment of solvation for molecular mechanics and dynamics, J. Am. Chem. Soc. 112 (1990) 6127–6129.
[31] J. Weiser, P.S. Shenkin, W.C. Still, Approximate atomic surfaces from linear combinations of pair-wise overlaps (LCPO), J. Comput. Chem. 20 (2) (1999) 217–230.
[32] T. Kawaguchi, S. Kato, K. Otsuka, G. Watanabe, T. Kumabe, T. Tominaga, T. Yoshimoto, C. Ishioka, The relationship among p53 oligomer formation, structure and transcriptional activity using a comprehensive missense mutation library, Oncogene 24 (46) (2005) 6976–6981.